THE JOURNAL OF PHYSICAL CHEMISTRY A

pubs.acs.org/JPCA

Article

A Theoretical Study of the Recently Suggested Mn^{VII} Mechanism for O−O Bond Formation in Photosystem II

Xi-Chen Li,* Jing Li, and Per E. M. Siegbahn*

Cite This: *J. Phys. Chem. A* 2020, 124, 8011−8018

Read Online

ACCESS | Metrics & More | Article Recommendations | Supporting Information

ABSTRACT: The mechanism for water oxidation in photosystem II has been a major topic for several decades. The active catalyst has four manganese atoms connected by bridging oxo bonds, in a complex termed the oxygen-evolving complex (OEC), which also includes a calcium atom. The O−O bond of oxygen is formed after absorption of four photons in a state of the OEC termed S_4. There has been essential consensus that in the S_4 state, all manganese atoms are in the Mn(IV) oxidation state. However, recently there has been a suggestion that one of the atoms is in the Mn(VII) state. In the present computational study, the feasibility of that proposal has been investigated. It is here shown that the mechanism involving Mn(VII) has a much higher barrier for forming O_2 than the previous proposal with four Mn(IV) atoms.

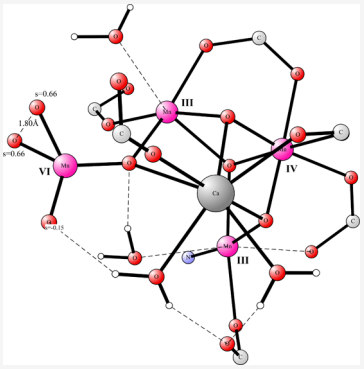

INTRODUCTION

Water oxidation using sunlight is one of the most important processes in nature.[1,2] Decades of research have been dedicated to find out how this remarkable reaction occurs. Large theoretical and experimental efforts have finally been able to reach a high level of consensus on even the finest details of the mechanism. The earliest X-ray structures were done only to a low resolution.[3,4] However, the structures of the four observable intermediates in the process, S_0 to S_3, have now been determined to high precision.[5−10] The most recent experimental determinations of the structures have been done using the X-ray free electron laser (X-FEL) technique. The structure of the oxygen-evolving complex (OEC) has long been known to contain four manganese atoms and a calcium held together by bridging oxo groups. The leading mechanisms for the O−O bond formation have initially circled around two main possibilities. For many years, one of the leading suggestions was that the O−O bond was formed by a nucleophilic water attack on a terminal oxo group bound to the OEC.[11−13] During more recent years, that mechanism has been criticized, both by theory and by experiments. Instead, the leading mechanism is now that the O−O bond is formed between a radical oxyl group and a bridging oxo ligand.[14−19] It can be added that there exists another suggestion for O−O bond formation with similarities to the present suggestion.[48] However, in that mechanism, an oxygen radical plays a major role in S_3, which is different from the mechanism suggested by us. Alternative suggestions have become more and more scarce. However, a new mechanism was recently suggested by Sun and Zhang[20] In that mechanism, the key step is the formation of a Mn(VII) di-oxo site on the dangling manganese in the S_4 state. The O−O bond should then be formed between the two oxo groups.

In the present paper, the Mn^{VII} mechanism by Sun and Zhang is compared to the previous consensus mechanism involving a bridging oxo and a terminal oxyl. That question is studied by using exactly the same theoretical techniques as have previously been used to successfully predict the structures of all the observable S states prior to, but later confirmed by, experiments.

COMPUTATIONAL DETAILS

The same methods and basis sets were used here as the ones used in previous similar studies.[16,21] The calculations start out by geometry optimizations using the DFT functional B3LYP.[22] The basis sets (LACVP*) used in these optimizations are of moderate size but have been shown to be adequate if just the energies are of interest.[23] Backbone atoms were fixed from the X-ray structure as described before.[24]

For the final energies, a large basis set was used with cc-pVTZ(−*f*) for the nonmetal atoms and with LACV3P+ for the metals. An important finding using B3LYP is that the energies are almost only sensitive to the fraction of exact exchange in the functional.[25] In previous studies of photosystem II (PSII),[16,26] it has been found that the fraction of 15% is the

Received: June 6, 2020
Revised: August 30, 2020
Published: September 2, 2020

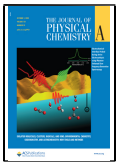

https://dx.doi.org/10.1021/acs.jpca.0c05135
J. Phys. Chem. A 2020, 124, 8011−8018

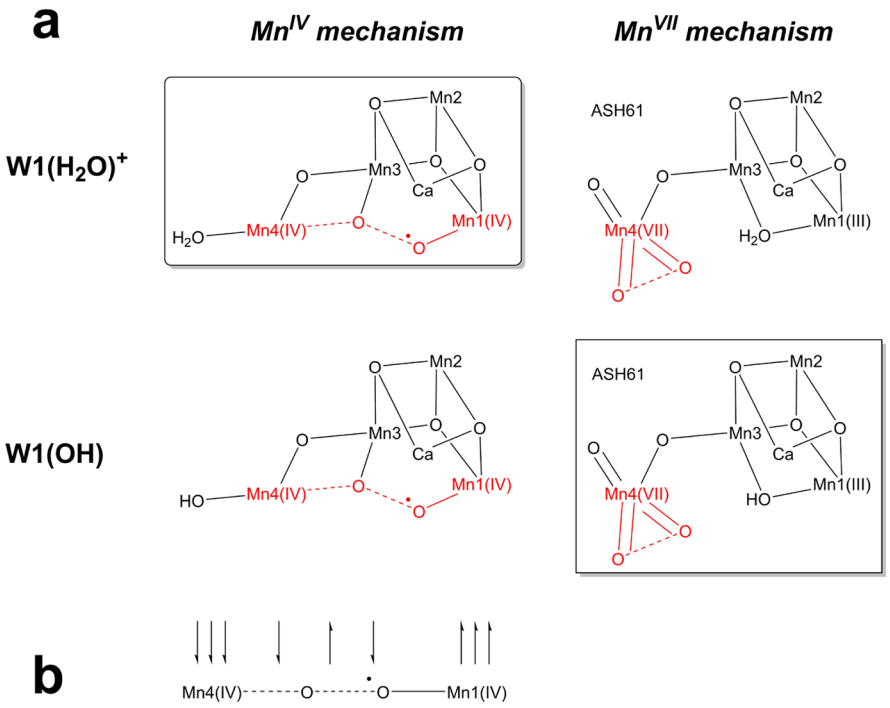

Figure 1. Chemical models and O−O bond formation mechanisms investigated in the present study. (a) Mn^{IV} mechanism and the Mn^{VII} mechanism for O−O bond formation, respectively, using the $W1(H_2O)^+$ model and the W1(OH) model of the OEC, respectively. The rectangles enclose the original suggestions in refs 16 and 20. (b) Key spin alignment in the Mn^{IV} mechanism to allow the low-barrier O−O bond formation.

one that reproduces the experimental redox potential best, and this fraction is therefore used also here. The D2 dispersion correction[27,28] was used as it was done in the previous study[16] for the final energies. Solvation effects were obtained using a Poisson−Boltzmann solver,[29] with a dielectric constant of 6.0. Zero-point effects were taken from frequency calculations on optimized structures. The best energy diagram for the entire water oxidation process in PSII is given in a review.[30] The energy diagram given in an earlier study[16] is only slightly different.

The experimentally known driving force for the entire water oxidation cycle is 41.5 kcal/mol. It is used to define the reference value for the transition energies. The energies for removing a (H^+, e^-) couple (the same in each transition) is then simply chosen to fit the experimental driving force. The value obtained in the present and previous studies is then 405.9 kcal/mol.[26] The details for all the transitions are described in detail in the same reference. It is important to note that the same value can be used independent of the model of the cluster and can therefore be used for both the $W1(H_2O)^+$ and W1(OH) models discussed below. This procedure for obtaining the energies was used to predict structures and energies for the S transitions, which were confirmed by experiments years later, thereby lending confidence to the procedure used.

The chemical models and O−O bond formation mechanisms investigated in the present study are given in Figure 1. Thus, O−O bond forms between the Mn(IV)-bound oxyl radical and an oxo bridge in the Mn^{IV} mechanism and between two Mn(VII)-bound oxo groups in the Mn^{VII} mechanism, respectively. Furthermore, the $W1(H_2O)^+$ model contains one proton more than the W1(OH) model, for example, at the Mn4(IV)-bound water site through the entirety of the Mn^{IV} mechanism and through S_0 to S_3 in the Mn^{VII} mechanism.

RESULTS

The recently suggested model for water oxidation will, in the following, be termed the W1(OH) model, while the previous model will be termed the $W1(H_2O)^+$ model (Figure 1). The core structure of the W1(OH) model for the S_0 state is shown in Figure 2. The starting S_0 structure has three Mn(III) and

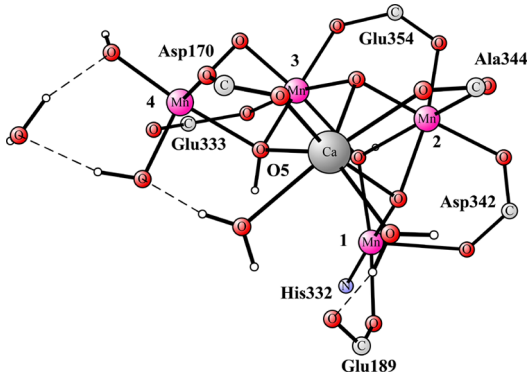

Figure 2. S_0 state for the suggested W1(OH) model. It differs from the previous $W1(H_2O)^+$ model only for the water-derived ligands bound to Mn4. In the W1(OH) model, they are two hydroxides, while in the $W1(H_2O)^+$ model they are one hydroxide and one water.

one Mn(IV). The computed energies for the $W1(H_2O)^+$ and W1(OH) models are shown in Table 1. The energies given for the $W1(H_2O)^+$ model are the same as those given earlier[30] (essentially the same as in Figure 2 with 15% exact exchange in ref 26 except for the corrections of 5 kcal/mol for S_2 to S_3 and S_3 to S_4). There is one important difference between the W1(OH) and $W1(H_2O)^+$ models. The $W1(H_2O)^+$ model has one water and one hydroxide on Mn4, while the W1(OH) model has one less proton and therefore two hydroxides on

https://dx.doi.org/10.1021/acs.jpca.0c05135
J. Phys. Chem. A 2020, 124, 8011−8018

Table 1. Calculated Energies (kcal/mol) for the W1(H_2O)$^+$ and W1(OH) Models[a]

transition	model	(H^+, e^-)	ΔE	mechanism
S_0 to S_1	W1(H_2O)$^+$	391.8	−14.1[a]	
	W1(OH)	385.4	−20.5	
S_1 to S_2	W1(H_2O)$^+$			
	W1(OH)			
S_2 to S_2	W1(H_2O)$^+$	399.5	−6.4[a]	
	W1(OH)	403.0	−2.8	
S_2 to S_4	W1(H_2O)$^+$	411.6	+5.7[a]	Mn^{IV}
	W1(H_2O)$^+$	451.2	+45.3[b]	Mn^{VII}
	W1(OH)	410.4	+4.5[c]	Mn^{IV}
	W1(OH)	439.7	+33.8[d]	Mn^{VII}
O−O TS in S_4	W1(H_2O)$^+$		+7.7[a]	Mn^{IV}
O−O TS in S_4	W1(H_2O)$^+$		+36	Mn^{VII}
O−O TS in S_4	W1(OH)		+6.8	Mn^{IV}
O−O TS in S_4	W1(OH)		+44	Mn^{VII}

[a]The W1(OH) model has one proton less than the W1(H_2O)$^+$ model. (H^+, e^-) shows the energy for removing a (H^+, e^-) couple, where the reference energy is 405.9 kcal/mol. ΔE shows the relative energy compared to the reference energy. (a): as given in the recent review;[30] (b): 45.3 kcal/mol = (43.0 − (6.2 − 2.8) + 5.7) kcal/mol, with the first two operands given in Table S1 in the Supporting Information and the third operand being the spin correction; (a,c): including a spin correction of −2.8 kcal/mol as discussed in the previous studies;[16,26] (d): 33.8 kcal/mol = (−10.2 − (−36.7 − 2.8) + 4.5) kcal/mol, with the first two operands given in Table S2 in the Supporting Information and the third operand being the spin correction.

Mn4. There is plenty of theoretical[16] and experimental evidence that there should be one water and one hydroxide on Mn4 as in the W1(H_2O)$^+$ model.[31] The presence of two hydroxides on Mn4 in the W1(OH) model was suggested[20] in order to reach the Mn(VII) state in S_4. For the early transitions, the different number of hydroxides on Mn4 is by far the most important difference between the models since, for the remaining part, the suggested W1(OH) model uses all known information deduced previously from theoretical modeling and from experiments for the S_0 to S_3 states. The release of protons and electrons, as always for redox enzymes, occurs in an alternating fashion. For PSII, the order follows from the experimental facts that only an electron leaves between S_1 and S_2,[32] while a proton leaves first in the S_2 to S_3 transition.[9,10,33−42] A proton leaves first also in the S_3 to S_4 transition.[33,34] The energies for the S transitions leading to S_4 are only reported using the respective models for each mechanism, the W1(H_2O)$^+$ model for the Mn^{IV} mechanism and the W1(OH) model for the Mn^{VII} mechanism. In the discussion on O−O bond formation, both models are used for both mechanisms.

S_0 to S_1. In the W1(H_2O)$^+$ model, Mn2 is the one that is Mn(IV) for S_0, while in the W1(OH) model it is Mn3, see Figure 2. For the W1(H_2O)$^+$ model, the transition from S_0 to S_1 by removing a (H^+, e^-) couple is exergonic by −14.1 kcal/mol, while with the W1(OH) model it is exergonic by −20.5 kcal/mol. This leads to the S_1 state, which has two Mn(IV). In the W1(H_2O)$^+$ model, they are Mn2,Mn3, while in the W1(OH) model they are Mn3,Mn4. The proton released in both models is the one on the central O5 atom. An important difference between the models is that a water is fairly strongly bound to Mn1 in S_1 by 9.8 kcal/mol in the W1(OH) model, while it is unbound in the W1(H_2O)$^+$ model. The experimental X-FEL structures do not have water at that position in S_1.

S_1 to S_2. This transition is different from the other ones. It has been shown by experiments that only an electron leaves in the transition,[32] while the proton leaves in the next transition.[9,10,33−42] For the W1(H_2O)$^+$ model, the electron released comes from Mn4, while for the W1(OH) model it comes from Mn2. In S_2, the oxidation states are thus the same for both models with only Mn1 being Mn(III).[42−46] The reason for this similarity is that Mn1 is five-coordinated in both models and is therefore the hardest one to oxidize.

Since the models differ in charge, it is not possible to directly compare the calculated energies for the release of the electron. This means that the parametrized reference value for the release of an electron only should optimally be different in the two models. The reason for this is that the value is sensitive to charges surrounding the model, which should be different in the models due to the different charges of the respective OECs. It is important to note that the reference value used for the release of a (H^+, e^-) couple should be approximately the same for the two models since it is only determined by the driving force for the entire catalytic cycle for water oxidation. Since the charge is the same before and after the release of the (H^+, e^-) couple, the value is not sensitive to long-range charges either. In S_2, the water on Mn1 is strongly bound to Mn1 by 8.6 kcal/mol in the W1(OH) model but slightly unbound in the W1(H_2O)$^+$ model. Again, no water is seen in the X-FEL structures of S_2.

S_2 to S_3. In this transition, the proton is known to be released first.[9,10,33−42] The proton released is for both models from the water on Mn1, and the electron released is for both models from Mn4. The combined (H^+, e^-) release is exergonic by −6.4 kcal/mol for the W1(H_2O)$^+$ model, while it is exergonic by −2.8 kcal/mol for the W1(OH) model.

S_3 to S_4. This is the last transition before O−O bond formation, and it is therefore particularly important. In the W1(H_2O)$^+$ model, both the proton and electron are released from the hydroxide on Mn1, leading to an oxyl radical. The release of a (H^+, e^-) couple is endergonic by +5.7 kcal/mol for the W1(H_2O)$^+$ model.[30] It should be noted that in that model, the initial proton release is endergonic by +2.1 kcal/mol, while the following electron release is endergonic by +3.6 kcal/mol. For the calculation of the rate-limiting barrier for O−O bond formation, the endergonicity of +5.7 kcal/mol will be added to the local barrier in S_4, see below, and is therefore the value given in Table 1. Since S_4 has not been observed experimentally, reaching S_4 should be endergonic, and the uphill energy of +5.7 kcal/mol is possible to overcome. The uphill energy would be more than compensated by the subsequent O−O bond formation step, which is more exergonic. To reach a Mn(VII) state with the W1(H_2O)$^+$ model requires another +39.6 kcal/mol, which means that a cost of 45.3 kcal/mol is needed to reach the Mn(VII) S_4 state in the W1(H_2O)$^+$ model, which makes it unreachable. For the W1(OH) model, the release of a (H^+, e^-) couple is endergonic by +4.5 kcal/mol. The S_4 structure reached is one with four Mn(IV) and one oxyl radical as in the Mn^{IV} mechanism. To reach the desired Mn(VII) state for the W1(OH) model in S_4 requires another +29.3 kcal/mol, which means that the Mn(VII) S_4 structure is as much +33.8 kcal/mol higher than S_3, which makes S_4 unreachable as well. Another very important difference is that the Mn(VII) S_4 structure lacks an oxyl radical, see further below.

https://dx.doi.org/10.1021/acs.jpca.0c05135
J. Phys. Chem. A 2020, 124, 8011−8018

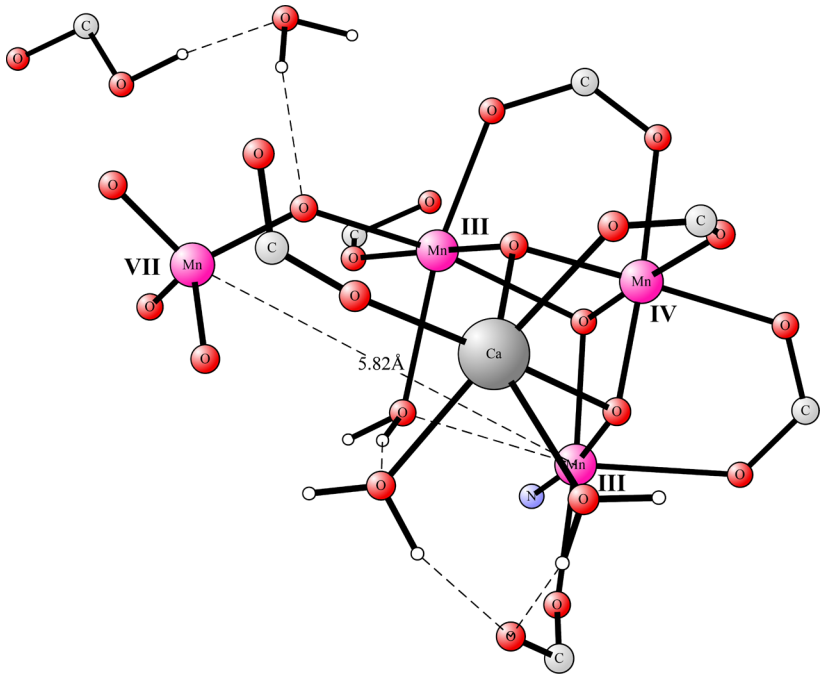

Figure 3. Optimized Mn(VII)=O S_4 state for the W1$(H_2O)^+$ model.

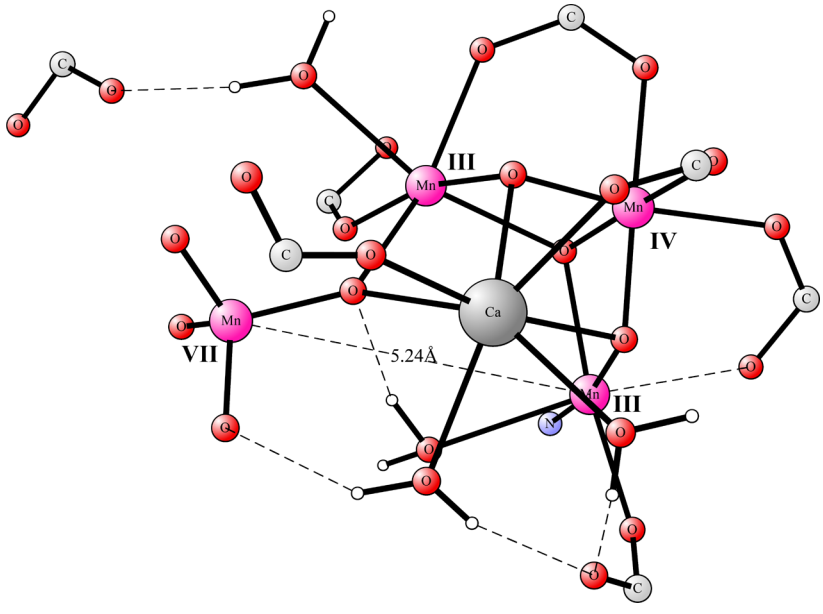

Figure 4. Optimized Mn(VII)=O S_4 state for the W1(OH) model, with one proton less than the optimal one of the W1$(H_2O)^+$ model.

O−O Bond Formation in S_4. In the Mn^{IV} mechanism,[14−16,47] O−O bond formation was suggested to be rate limiting and should occur between an oxyl radical and an oxo bridge, both inside the cavity. In the Mn^{VII} mechanism,[20] oxygen evolution in S_4 to S_0 was suggested to be rate limited by the slow charge rearrangement going from Mn(IV,IV,IV,IV) with $Y_Z^{\bullet}$ to Mn(III,III,IV,VII). The O−O bond formation should then occur rapidly by direct coupling between two terminal oxo groups bound to the dangling Mn4(VII).

Because the two suggested models for the mechanisms differ by one proton and therefore by one charge, the first comparison was made between the lowest energy Mn(IV)−$O^{\cdot-}$ and Mn(VII)=O structures for each overall charge, respectively.

For the overall charge originally suggested in the Mn^{IV} mechanism,[16] the lowest energy Mn(IV)−$O^{\cdot-}$ structure is the same as previously reported.[26] The lowest energy Mn(VII)=O structure optimized for the same overall charge is shown in Figure 3. The Mn oxidation states obtained are Mn(III,IV,III,VII). The spins are 3.92, 2.99, 3.84, and 0.04, respectively, typical for these oxidation states. The energy of the Mn(VII)=O structure is +39.6 kcal/mol higher in energy than that of the Mn(IV)−$O^{\cdot-}$ structure with the same number of atoms and electrons, see above. The dangling Mn4(VII) center is tetrahedrally coordinated by four oxo groups, three of which are terminal ligands. The fourth oxo group is coordinated to both Mn4(VII) and Mn3(III), ligating along the Jahn−Teller axis of Mn3. There is one water inside the

https://dx.doi.org/10.1021/acs.jpca.0c05135
J. Phys. Chem. A 2020, 124, 8011−8018

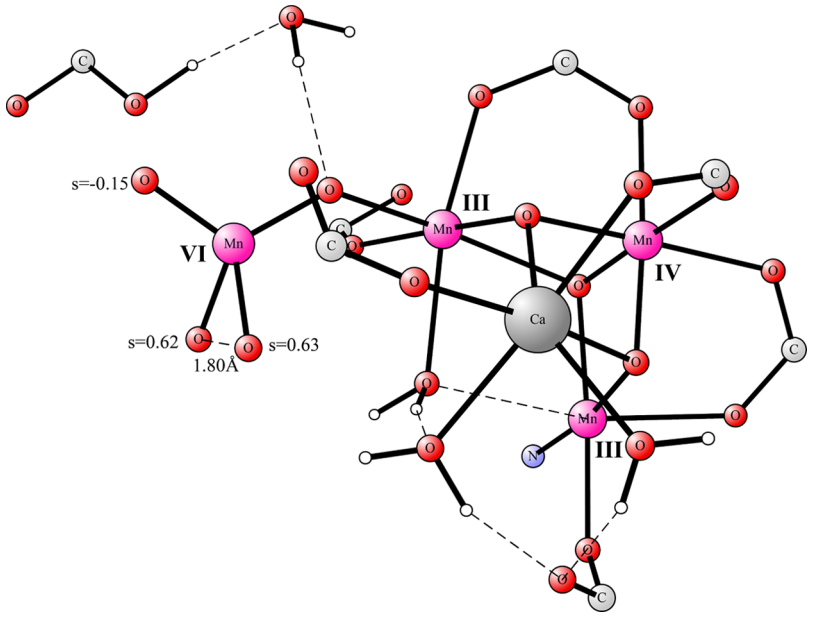

Figure 5. Approximate TS for O−O bond formation with a Mn(VII) reactant for a model with the same number of protons as for the one optimal for the Mn^{IV} mechanism.

cavity, which is bound to Mn3(III). The carboxylate group of Asp61 is protonated at the trans position and donates a hydrogen bond to a nearby water molecule. The alternative conformer where Asp61 is protonated at the cis position and donates a hydrogen bond directly to a terminal oxo ligand of Mn4(VII) is 43.8 kcal/mol higher in energy than the Mn(IV)−$O^{\cdot-}$structure. In this conformer, Mn3(III) has a pentagonal bipyramidal coordination, probably because of the hydrogen bond from Asp61 to the Mn4(VII)-bound oxo. The conformer with a protonation at the cis position of Asp61 and with an octahedral Mn3(III) is 51.4 kcal/mol higher in energy than the Mn(IV)−$O^{\cdot-}$structure.

For the overall charge originally suggested in the Mn^{VII} mechanism with one proton less,[20] the lowest energy Mn(IV)−$O^{\cdot-}$structure was obtained on the basis of the Mn(IV)−$O^{\cdot-}$structure previously reported[26] by removing a proton from the water molecule bound to the dangling Mn4(IV) trans to the cavity. The lowest energy Mn(VII)═O structure optimized for the same overall charge is shown in Figure 4. The Mn oxidation states obtained are Mn-(III,IV,III,VII), rather than Mn(III,III,IV,VII) as previously suggested.[20] The energy of the Mn(VII)═O structure is +29.3 kcal/mol higher in energy than that of the Mn(IV)−$O^{\cdot-}$structure with the same number of atoms and electrons. Compared to the Mn(VII)═O structure with one more proton (Figure 3), the tetrahedral Mn4(VII) is 0.58 Å closer to Mn1(III) because the oxo bridging Mn4(VII) and Mn3(III) moves further inside the cavity. The carboxylate Asp61 is not protonated but stabilized by hydrogen bonds donated by water molecules. The alternative protonation state, with a protonated Asp61 and a hydroxide inside the cavity, is 35.5 kcal/mol higher in energy than the Mn(IV)−$O^{\cdot-}$structure. The Mn oxidation states obtained are (III,IV,III,VII). The alternative solution with the Mn oxidation states of (III,III,IV,VII), thereby resembling the Mn(VII)═O species previously proposed,[20] is 40.3 kcal/mol higher in energy than the Mn(IV)−$O^{\cdot-}$structure.

O−O bond formation in the S_4 state of the Mn^{IV} mechanism and the Mn^{VII} mechanism was examined. For the W1$(H_2O)^+$ model where the dangling Mn4(IV) has one water ligand near Asp-61, the lowest energy reactive complex contains a high-spin Mn1(IV)-bound oxyl radical. The lowest barrier TS for O−O bond formation is a direct coupling between the oxyl radical bound to the high-spin Mn1(IV) and an oxo bridge, as published previously.[16,26,30] The calculated barrier for that mechanism was 13.4 kcal/mol,[30] with respect to the S_3 state. As described above, the conformer with the same number of electrons and protons but a closed-shell Mn(VII), tetrahedrally coordinated by four oxo anions, is +39.6 kcal/mol higher than the solution with a high-spin Mn1(IV)-bound oxyl radical. The TS for O−O bond formation via coupling between two oxo groups bound to the closed-shell Mn(VII), as suggested in the recent paper,[20] was approximated by a reaction coordinate scan. The approximate TS structure is shown in Figure 5. The local barrier, counted from the conformer with the closed-shell Mn(VII), was found to be around 36 kcal/mol, which means an overall barrier of 81 (= 5.7 + 39.6 + 36) kcal/mol, with respect to the S_3 state. The high barrier can be partly explained by the lack of an oxyl radical for the S_4 reactant.

For the W1(OH) model, where the dangling Mn4(IV) has two hydroxide ligands, one of them near Asp-61, the lowest energy reactive complex is still a conformer that contains a high-spin Mn1(IV)-bound oxyl radical. For the Mn^{IV} mechanism, now with one proton less, the local barrier is only 6.8 kcal/mol, actually lower than that for the regular mechanism with one proton more. If the energy cost of +4.5 kcal/mol going from the S_3 to the S_4 state using the W1(OH) model is included, then the total barrier becomes 11.3 kcal/mol, about 2 kcal/mol lower than that for the regular mechanism with one proton more. As described above in this subsection, the conformer with the same number of electrons and protons but a closed-shell Mn(VII), tetrahedrally coordinated by four oxo anions, is 29.3 kcal/mol higher than the solution with a high-spin Mn1(IV)-bound oxyl radical. The TS for O−O bond formation via coupling between two oxo

https://dx.doi.org/10.1021/acs.jpca.0c05135
J. Phys. Chem. A 2020, 124, 8011−8018

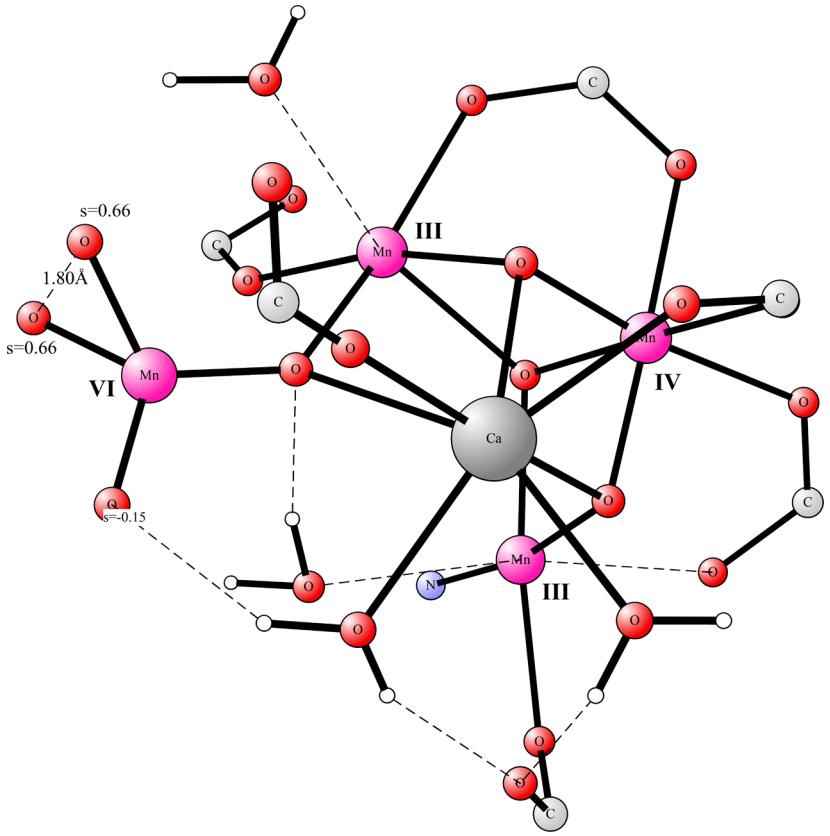

Figure 6. Approximate TS for O−O bond formation with a Mn(VII) reactant for a model with one proton less than for the one optimal for the Mn^{IV} mechanism.

groups bound to the closed-shell Mn(VII) was also approximated by a reaction coordinate scan. The approximate TS structure is shown in Figure 6. The local barrier, counted from the conformer with the closed-shell Mn(VII), was found to be around 44 kcal/mol, which means an overall barrier of 78 (= 4.5 + 29.3 + 44) kcal/mol. Again, the lack of an oxyl radical can partly explain the very high barrier. It should here be emphasized that we have strictly followed the suggestion in the recent paper on the Mn^{VII} mechanism[20] with a TS coupling two oxo groups. With a reshuffling of the protons and a change of oxidation states prior to O−O bond formation, the TS would, of course, go over to the one for the Mn^{IV} mechanism.

SUMMARY

The recently suggest mechanism involving Mn(VII) has been studied and compared to the previous mechanism, where the manganese atoms never reach an oxidation state higher than IV. For the S transitions from S_0 to S_3, there are relatively small energy differences between the mechanisms. It should be noted that this only concerns oxidations in which both an electron and a proton are released. For oxidations where only an electron leaves, the differences are likely to be much larger since the charges of the clusters are different in the two models, but those energy differences are hard to estimate due to the different charge distributions of the OEC and its surrounding in the two mechanisms.

In the final S transition from S_3 to S_4, the difference between the mechanisms becomes substantial even for the release of a (H^+, e^-) couple. Reaching the S_4 state, for the structures optimal for the Mn^{IV} mechanism, is only endergonic by +5.7 kcal/mol in the Mn^{IV} mechanism;[16] while in the Mn^{VII} mechanism, for the structures optimal for the Mn^{VII} mechanism with one proton less, the energy cost is +33.8 kcal/mol to reach the desired S_4 state with one Mn(VII). For the Mn^{IV} mechanism, the barrier from the S_3 reference state is 13.4 kcal/mol. In the Mn^{VII} mechanism, it is as high as 78 kcal/mol.

In summary, for both models, the structures in the Mn^{VII} mechanism have much higher energies than the ones in the Mn^{IV} mechanism. The appearance of the Mn(VII)═O oxidation states, Mn(III,III,IV,VII) or Mn(III,IV,III,VII), is very unlikely to be significant in the oxygen evolution in the OEC. In addition, the local barriers for O−O bond formation starting from the closed-shell Mn4(VII)═O are estimated to be around +36 and + 44 kcal/mol, respectively, which are much higher than the value in the Mn^{IV} mechanism of +7.7 kcal/mol, as previously reported.[26]

ASSOCIATED CONTENT

Supporting Information

The Supporting Information is available free of charge at https://pubs.acs.org/doi/10.1021/acs.jpca.0c05135.

Coordinates for the structures for the Mn^{VII} mechanism (PDF)

AUTHOR INFORMATION

Corresponding Authors

Xi-Chen Li − *College of Chemistry, Beijing Normal University, Beijing 100875, China;* orcid.org/0000-0002-1643-4327; Email: li_xi_chen@hotmail.com

https://dx.doi.org/10.1021/acs.jpca.0c05135
J. Phys. Chem. A 2020, 124, 8011−8018

Per E. M. Siegbahn − *Department of Organic Chemistry, Arrhenius Laboratory, Stockholm University, SE-106 91 Stockholm, Sweden;* orcid.org/0000-0001-7787-1881; Email: per.siegbahn@su.se

Author

Jing Li − *College of Chemistry, Beijing Normal University, Beijing 100875, China*

Complete contact information is available at: https://pubs.acs.org/10.1021/acs.jpca.0c05135

Notes

The authors declare no competing financial interest.

■ ACKNOWLEDGMENTS

This work was supported by the National Natural Science Foundation of China (grant 21503018, 21571019, and 21573020), the Swedish Research Council, and the Knut and Alice Wallenberg Foundation. Computer time was generously provided by the Swedish National Infrastructure for Computing.

■ REFERENCES

(1) Lubitz, W.; Chrysina, M.; Cox, N. Water Oxidation in Photosystem II. *Photosynth. Res.* **2019**, *142*, 105−125.
(2) Cox, N.; Pantazis, D. A.; Lubitz, W. Current Understanding of the Mechanism of Water Oxidation in Photosystem II and Its Relation to XFEL Data. *Annu. Rev. Biochem.* **2020**, *89*, 795−820.
(3) Ferreira, K. N.; Iverson, T. M.; Maghlaoui, K.; Barber, J.; Iwata, S. Architecture of the Photosynthetic Oxygen-Evolving Center. *Science* **2004**, *303*, 1831.
(4) Loll, B.; Kern, J.; Saenger, W.; Zouni, A.; Biesiadka, J. Towards Complete Cofactor Arrangement in the 3.0°A Resolution Structure of Photosystem II. *Nature* **2005**, *438*, 1040−1044.
(5) Umena, Y.; Kawakami, K.; Shen, J.-R.; Kamiya, N. Crystal Structure of Oxygen- Evolving Photosystem II at a Resolution of 1.9 Å. *Nature* **2011**, *473*, 55−60.
(6) Suga, M.; Akita, F.; Hirata, K.; Ueno, G.; Murakami, H.; Nakajima, Y.; Shimizu, T.; Yamashita, K.; Yamamoto, M.; Ago, H.; et al. Native Structure of Photosystem II at 1.95 Å Resolution Viewed by Femtosecond X-Ray Pulses. *Nature* **2015**, *517*, 99−103.
(7) Young, I. D.; Ibrahim, M.; Chatterjee, R.; Gul, S.; Fuller, F. D.; Koroidov, S.; Brewster, A. S.; Tran, R.; Alonso-Mori, R.; Kroll, T.; et al. Structure of Photosystem II and Substrate Binding at Room Temperature. *Nature* **2016**, *540*, 453−457.
(8) Suga, M.; Akita, F.; Sugahara, M.; Kubo, M.; Nakajima, Y.; Nakane, T.; Yamashita, K.; Umena, Y.; Nakabayashi, M.; Yamane, T.; et al. Light-Induced Structural Changes and the Site of O=O Bond Formation in PSII Caught by XFEL. *Nature* **2017**, *543*, 131−135.
(9) Kern, J.; Chatterjee, R.; Young, I. D.; Fuller, F. D.; Lassalle, L.; Ibrahim, M.; Gul, S.; Fransson, T.; Brewster, A. S.; Alonso-Mori, R.; et al. Structures of the Intermediates of Kok's Photosynthetic Water Oxidation Clock. *Nature* **2018**, *563*, 421−425.
(10) Ibrahim, M.; Fransson, T.; Chatterjee, R.; Cheah, M. H.; Hussein, R.; Lassalle, L.; Sutherlin, K. D.; Young, I. D.; Fuller, F. D.; Gul, S.; et al. Untangling the Sequence of Events during the S2 → S3 Transition in Photosystem II and Implications for the Water Oxidation Mechanism. *Proc. Natl. Acad. Sci. U. S. A.* **2020**, *117*, 12624.
(11) Sproviero, E. M.; Gascón, J. A.; McEvoy, J. P.; Brudvig, G. W.; Batista, V. S. Quantum Mechanics/Molecular Mechanics Study of the Catalytic Cycle of Water Splitting in Photosystem II. *J. Am. Chem. Soc.* **2008**, *130*, 3428−3442.
(12) Sproviero, E. M.; Gascón, J. A.; McEvoy, J. P.; Brudvig, G. W.; Batista, V. S. A Model of the Oxygen-Evolving Center of Photosystem II Predicted by Structural Refinement Based on EXAFS Simulations. *J. Am. Chem. Soc.* **2008**, *130*, 6728−6730.
(13) McEvoy, J. P.; Brudvig, G. W. Water-Splitting Chemistry of Photosystem II. *Chem. Rev.* **2006**, *106*, 4455−4483.
(14) Siegbahn, P. E. M. O−O Bond Formation in the S_4 State of the Oxygen-Evolving Complex in Photosystem II. *Chem. − Eur. J.* **2006**, *12*, 9217−9227.
(15) Siegbahn, P. E. M. Structures and Energetics for O_2 Formation in Photosystem II. *Acc. Chem. Res.* **2009**, *42*, 1871−1880.
(16) Siegbahn, P. E. M. Water Oxidation Mechanism in Photosystem II, Including Oxidations, Proton Release Pathways, O − O Bond Formation and O_2 Release. *Biochim. Biophys. Acta, Bioenerg.* **2013**, *1827*, 1003−1019.
(17) Suga, M.; Akita, F.; Yamashita, K.; Nakajima, Y.; Ueno, G.; Li, H.; Yamane, T.; Hirata, K.; Umena, Y.; Yonekura, S.; et al. An Oxyl/Oxo Mechanism for Oxygen- Oxygen Coupling in PSII Revealed by an X-Ray Free-Electron Laser. *Science* **2019**, *366*, 334.
(18) Yamaguchi, K.; Yamanaka, S.; Isobe, H.; Shoji, M.; Miyagawa, K.; Nakajima, T.; Kawakami, T.; Okumura, M. Theoretical and Computational Investigations of Geometrical, Electronic and Spin Structures of the $CaMn_4O_X$ (X = 5, 6) Cluster in the Kok Cycle S_i (i = 0−3) of Oxygen Evolving Complex of Photosystem II. *Physiol. Plant.* **2019**, *166*, 44−59.
(19) Corry, T. A.; O'Malley, P. J. Electronic−Level View of O−O Bond Formation in Nature's Water Oxidizing Complex. *J. Phys. Chem. Lett.* **2020**, *11*, 4221−4225.
(20) Zhang, B.; Sun, L. Why Nature Chose the Mn4CaO5 Cluster as Water-Splitting Catalyst in Photosystem II: A New Hypothesis for the Mechanism of O−O Bond Formation. *Dalton Trans.* **2018**, *47*, 14381−14387.
(21) Blomberg, M. R. A.; Borowski, T.; Himo, F.; Liao, R.-Z.; Siegbahn, P. E. M. Quantum Chemical Studies of Mechanisms for Metalloenzymes. *Chem. Rev.* **2014**, *114*, 3601−3658.
(22) Becke, A. D. Density-functional Thermochemistry. III. The Role of Exact Exchange. *J. Chem. Phys.* **1993**, *98*, 5648−5652.
(23) Siegbahn, P. E. M. Modeling Aspects of Mechanisms for Reactions Catalyzed by Metalloenzymes. *J. Comput. Chem.* **2001**, *22*, 1634−1645.
(24) Siegbahn, P. E. M. The Effect of Backbone Constraints: The Case of Water Oxidation by the Oxygen-Evolving Complex in PSII. *ChemPhysChem* **2011**, *12*, 3274−3280.
(25) Siegbahn, P. E. M.; Blomberg, M. R. A. A Systematic DFT Approach for Studying Mechanisms of Redox Active Enzymes. *Front. Chem.* **2018**, *6*, 644.
(26) Siegbahn, P. E. M.; Blomberg, M. R. A. Energy Diagrams for Water Oxidation in Photosystem II Using Different Density Functionals. *J. Chem. Theory Comput.* **2014**, *10*, 268−272.
(27) Grimme, S. Semiempirical GGA-Type Density Functional Constructed with a Long- Range Dispersion Correction. *J. Comput. Chem.* **2006**, *27*, 1787−1799.
(28) Grimme, S.; Antony, J.; Ehrlich, S.; Krieg, H. A Consistent and Accurate Ab Initio Parametrization of Density Functional Dispersion Correction (DFT-D) for the 94 Elements H-Pu. *J. Chem. Phys.* **2010**, *132*, 154104.
(29) Bochevarov, A. D.; Harder, E.; Hughes, T. F.; Greenwood, J. R.; Braden, D. A.; Philipp, D. M.; Rinaldo, D.; Halls, M. D.; Zhang, J.; Friesner, R. A. Jaguar: A High-Performance Quantum Chemistry Software Program with Strengths in Life and Materials Sciences. *Int. J. Quantum Chem.* **2013**, *113*, 2110−2142.
(30) Siegbahn, P. E. M. Water Oxidation by PSII: A Quantum Chemical Approach. In *Mechanisms of Primary Energy Transduction in Biology*; Wikström, M., Ed.; The Royal Society of Chemistry: 2018; pp. 273−295.
(31) Ames, W.; Pantazis, D. A.; Krewald, V.; Cox, N.; Messinger, J.; Lubitz, W.; Neese, F. Theoretical Evaluation of Structural Models of the S2 State in the Oxygen Evolving Complex of Photosystem II: Protonation States and Magnetic Interactions. *J. Am. Chem. Soc.* **2011**, *133*, 19743−19757.
(32) Förster, V.; Junge, W. Stoichiometry and Kinetics of Proton Release upon Photosynthetic Water Oxidation. *Photochem. Photobiol.* **1985**, *41*, 183−190.

(33) Rappaport, F.; Blanchard-Desce, M.; Lavergne, J. Kinetics of Electron Transfer and Electrochromic Change during the Redox Transitions of the Photosynthetic Oxygen- Evolving Complex. *Biochim. Biophys. Acta, Bioenerg.* **1994**, *1184*, 178−192.
(34) Haumann, M.; Liebisch, P.; Müller, C.; Barra, M.; Grabolle, M.; Dau, H. Photosynthetic O2 Formation Tracked by Time-Resolved X-Ray Experiments. *Science* **2005**, *310*, 1019.
(35) Siegbahn, P. E. M. The S2 to S3 Transition for Water Oxidation in PSII (Photosystem II). *Revisited. Phys. Chem. Chem. Phys.* **2018**, *20*, 22926−22931.
(36) Kim, C. J.; Debus, R. J. One of the Substrate Waters for O2 Formation in Photosystem II Is Provided by the Water-Splitting Mn4CaO5 Cluster's Ca^{2+} Ion. *Biochemistry* **2019**, *58*, 3185−3192.
(37) Chrysina, M.; Heyno, E.; Kutin, Y.; Reus, M.; Nilsson, H.; Nowaczyk, M. M.; DeBeer, S.; Neese, F.; Messinger, J.; Lubitz, W.; et al. Five-Coordinate MnIV Intermediate in the Activation of Nature's Water Splitting Cofactor. *Proc. Natl. Acad. Sci. U. S. A.* **2019**, *116*, 16841.
(38) Chrysina, M.; de Mendonça Silva, J. C.; Zahariou, G.; Pantazis, D. A.; Ioannidis, N. Proton Translocation via Tautomerization of Asn298 During the S2−S3 State Transition in the Oxygen-Evolving Complex of Photosystem II. *J. Phys. Chem. B* **2019**, *123*, 3068−3078.
(39) Krewald, V.; Neese, F.; Pantazis, D. A. Implications of Structural Heterogeneity for the Electronic Structure of the Final Oxygen-Evolving Intermediate in Photosystem II. *J. Inorg. Biochem.* **2019**, *199*, 110797.
(40) Zaharieva, I.; Dau, H. Energetics and Kinetics of S-State Transitions Monitored by Delayed Chlorophyll Fluorescence. *Front. Plant Sci.* **2019**, *10*, 386.
(41) Takemoto, H.; Sugiura, M.; Noguchi, T. Proton Release Process during the S2-to-S3 Transition of Photosynthetic Water Oxidation As Revealed by the pH Dependence of Kinetics Monitored by Time-Resolved Infrared Spectroscopy. *Biochemistry* **2019**, *58*, 4276−4283.
(42) Corry, T. A.; O'Malley, P. J. Molecular Identification of a High-Spin Deprotonated Intermediate during the S2 to S3 Transition of Nature's Water-Oxidizing Complex. *J. Am. Chem. Soc.* **2020**, *142*, 10240−10243.
(43) Boussac, A. Temperature Dependence of the High-Spin S_2 to S_3 Transition in Photosystem II: Mechanistic Consequences. *Biochim. Biophys. Acta, Bioenergy* **2019**, *1860*, 508−518.
(44) Chatterjee, R.; Lassalle, L.; Gul, S.; Fuller, F. D.; Young, I. D.; Ibrahim, M.; de Lichtenberg, C.; Cheah, M. H.; Zouni, A.; Messinger, J.; et al. Structural Isomers of the S2 State in Photosystem II: Do They Exist at Room Temperature and Are They Important for Function? *Physiol. Plant.* **2019**, *166*, 60−72.
(45) Corry, T. A.; O'Malley, P. J. Proton Isomers Rationalize the High- and Low-Spin Forms of the S2 State Intermediate in the Water-Oxidizing Reaction of Photosystem II. *J. Phys. Chem. Lett.* **2019**, *10*, 5226−5230.
(46) Taguchi, S.; Noguchi, T.; Mino, H. Molecular Structure of the S2 State with a g = 5 Signal in the Oxygen Evolving Complex of Photosystem II. *J. Phys. Chem. B* **2020**, *124*, 5531−5537.
(47) Siegbahn, P. E. M. Nucleophilic Water Attack Is Not a Possible Mechanism for O−O Bond Formation in Photosystem II. *Proc. Natl. Acad. Sci. U. S. A.* **2017**, *114*, 4966.
(48) Messinger, J. Evaluation of Different Mechanistic Proposals for Water Oxidation in Photosynthesis on the Basis of Mn4OxCa Structures for the Catalytic Site and Spectroscopic Data. *Phys. Chem. Chem. Phys.* **2004**, *6*, 4764−4771.

https://dx.doi.org/10.1021/acs.jpca.0c05135
J. Phys. Chem. A 2020, 124, 8011−8018